Transition Met Chem (2011) 36:521–530
DOI 10.1007/s11243-011-9498-7

Silica aerogel–iron oxide nanocomposites: recoverable catalysts for the oxidation of alcohols with hydrogen peroxide

Shahla Masoudian · Hassan Hosseini Monfared · Alireza Aghaei

Received: 1 March 2011 / Accepted: 27 April 2011 / Published online: 12 May 2011

Abstract Various aerogels of silica gel doped with Fe_2O_3 were prepared by sol–gel method. They were calcined to produce nanoparticle solids. The nanosized mixed oxides were active in the oxidation of alcohols and produced carbonyl compounds in very good to excellent yields using hydrogen peroxide.

Keywords Oxidation · Alcohols · Hydrogen peroxide · Sol–gel · Nanosized iron oxide-silica mixed oxides

Introduction

Iron-based materials are of great technological importance for their use in magnetic recording media, pigments, optics, ferro-fluids, magneto-optic devices, biology, and in catalysis [1–3]. Iron oxide/silica, Fe_2O_3/SiO_2, nanocomposites have recently attracted increasing attention due to their interesting properties and applications in sensing, catalysis, and magnetism [4–6]. Properties of Fe_2O_3/SiO_2 materials depend on the nature of the interaction between iron oxide and silica [7]. However, for most applications, effective composites must show the size of the particles in the nanometer range, porous texture of high surface area, and thermal stability [8–10].

Composites with different oxide/silica ratios and forms have synthesized with various methods for diverse applications, including via a formamide modified sol–gel process [11], Fe_2O_3/SiO_2 hollow spheres [12], iron oxide–silica nanocomposite films by spin coating as humidity sensors [13], mesoporous iron oxide–silica aerogels as catalysts for oxidation of NH_3 and reduction of NO [14], Fe–Si mixed oxide nanocomposites that contain iron oxide as the major phase [15], nanocluster iron oxide–silica aerogel catalysts for methanol partial oxidation [16], Fe_2O_3–SiO_2 composites, nanosized γ-Fe_2O_3 particles and study on the influence of the iron salts concentration [17], iron oxide–silica nanocomposites with wet impregnation [18], magnetic susceptibility studies of Fe_2O_3–SiO_2 [19], Fe_2O_3/SiO_2 nanocomposites based on fumed silica (S_{BET} = 265–337 m^2/g) [20], study of the magnetic properties of the iron oxide particles hosted in silica aerogels pores [21], silica aerogel–iron oxide nanocomposites as catalysts in conjugate additions and in the Biginelli reaction [22]. In spite of these studies, to the best of our knowledge, there is no report on the oxidation of alcohols by silica–iron oxide nanocomposites.

Oxidation of alcohols to aldehydes and ketones is one of the widely used chemical transformations in organic synthesis as these products are important precursors or intermediates in the synthesis of many drugs, vitamins, and fragrances [23–26]. A number of methods are known for alcohol oxidation [27]; however, the development of newer methods and methodologies is gaining much attention currently due to the significance of this reaction. Even though various methods are now known, the most common methods still use toxic, corrosive, and expensive oxidants such as chromium(VI) and manganese complexes, stringent conditions of high pressure or temperatures and use of strong mineral acids [28, 29]. The quest for clean and selective oxidation processes is continuing [30, 31]. Oxidation over metal catalysts using eco-friendly oxidants

S. Masoudian · H. Hosseini Monfared (✉)
Department of Chemistry, Zanjan University,
45195-313 Zanjan, Iran
e-mail: monfared@znu.ac.ir; monfared_2@yahoo.com
URL: http://www.znu.ac.ir/members/hosseini_hassan

A. Aghaei
Materials and Energy Research Center, 14155-4777 Tehran, Iran

such as hydrogen peroxide and molecular oxygen are preferred now for environmental and economical benefits. In spite of the advantages of H_2O_2 as a cheap and benign oxidant, its catalytic application has some limitations due to decomposition of H_2O_2 by traces of transition metal ions [32, 33]. Immobilization of iron on silica gel [34] or γ-alumina [35] considerably retards the non-productive decomposition of H_2O_2. Development in this area is based on different strategies with the aim of designing selective, stable, and high turnover catalytic systems.

The selectivity pattern and the formation rates of the reaction products provide information on the surface nature and dispersion of active sites at the molecular level [36]. Iron oxide itself exhibits strong acidic and weak redox properties [37]. Most known iron oxide–silica catalysts were prepared with iron nitrate or iron acetylacetonate and with nitrogen-containing bases as gelation agents [14].

The present study aims to employ sol–gel synthesis of iron alkoxide in isopropanol at the molecular level and to investigate the catalytic reactivity of silica-coordinated iron oxide aerogels. We wish to report an efficient protocol in which H_2O_2 has been used as the oxidizing agent in the presence of nanoparticles of Fe_2O_3–SiO_2 for the chemoselective oxidation of alcohols to their carbonyl compounds in high chemical yield and short reaction times. We have restricted ourselves to the use of hydrogen peroxide as the terminal oxidant. This oxidant is cheap, clean, and gives water as the sole byproduct [38].

Results and discussion

Characterization of the Fe_2O_3–SiO_2 catalysts

A series of nanosize iron oxide–silica aerogel catalysts were prepared via sol–gel methods. The homogeneous samples obtained under acidic conditions did not show any apparent gelation. In this case, the supercritical evaporation of the solvent is a fundamental process for obtaining a transparent gel. Samples were then dried in an autoclave. Finally, samples were calcined at 500 °C for 2 h or 10 min and alternatively at 100 °C for 10 min in air flow.

Table 1 presents a summary of all aerogels evaluated as catalysts for this work. The weight percent of iron is given as the sample composition. The 2 wt% of Fe (Fe_2O_3–SiO_2) aerogel is in the form of reddish brown powder with BET surface area of 555 m^2/g. Figure 1 is a field emission scanning electron micrograph for the 2 wt% of Fe iron oxide–silica aerogel after it was treated at 500 °C for 2 h (a), at 500 °C for 10 min (b), and at 100 °C for 10 min (c). The sample **1** silica-supported iron oxide calcined at 500 °C for 2 h (Fig. 1a) appears monolithic. Calcination at lower temperature and/or for a short time resulted to smaller size particles. In Fig. 1b and c, the SEM images of nanoparticles of iron oxide–silica aerogel catalysts after calcinations at 500 and 100 °C for 10 min are shown, respectively. Uniform and tiny particles almost spherical in shape, having sizes 63% between about 80–110 nm for Fig. 1b and 70% between about 50–80 nm for Fig. 1c, are observed.

Figure 2 shows X-ray diffraction (XRD) patterns of two aerogels after they were treated at 500 °C for 10 min. According these patterns, hematite (α-Fe_2O_3) was determined as the main crystalline phase in the 4.35 and 9.6 wt% Fe (Fe_2O_3–SiO_2) powders. The broadening near the peak baseline suggests the presence of very small crystallites (a few nanometers) [39]. XRD analyses indicated that all aerogels were mainly amorphous, a feature that is a reasonable indication that Fe_2O_3 is well dispersed in the silica matrix [40]. The aerogel sample showed the presence of traces of hematite in diffraction pattern of sample **3** (peaks at 31.88° and 45.58° in 2θ). For the sample **3**, the broad peak at $2\theta = 21-27^\circ$ is typically characteristic of amorphous silica. No evidence indicated the presence of maghemite or magnetite phases [41]. Empirically, iron oxide made from an alkoxide precursor similar in nature to the one we used exhibits a hematite phase at 500 °C as determined by XRD analysis [42].

Table 1 Structural properties of aerogels

Aerogel[a]	Surface area by BET (m^2/g)[b]	Particle size by SEM (nm)[b]
2 wt% of Fe (Fe_2O_3–SiO_2)[a]	555	63% between 80 and 110 nm
		70% between 50 and 80 nm[c]
4.35 wt% of Fe (Fe_2O_3–SiO_2)	580	61% between 200 and 250 nm
	(Mean pore diameter 11.20 nm)	
9.6 wt% of Fe (Fe_2O_3–SiO_2)	533	
	(Mean pore diameter 9.18 nm)	

[a] Weight percent-based sample composition

[b] Measurements were taken for aerogels after being treated in air for 10 min at 500 °C

[c] Calcined at 100 °C for 10 min

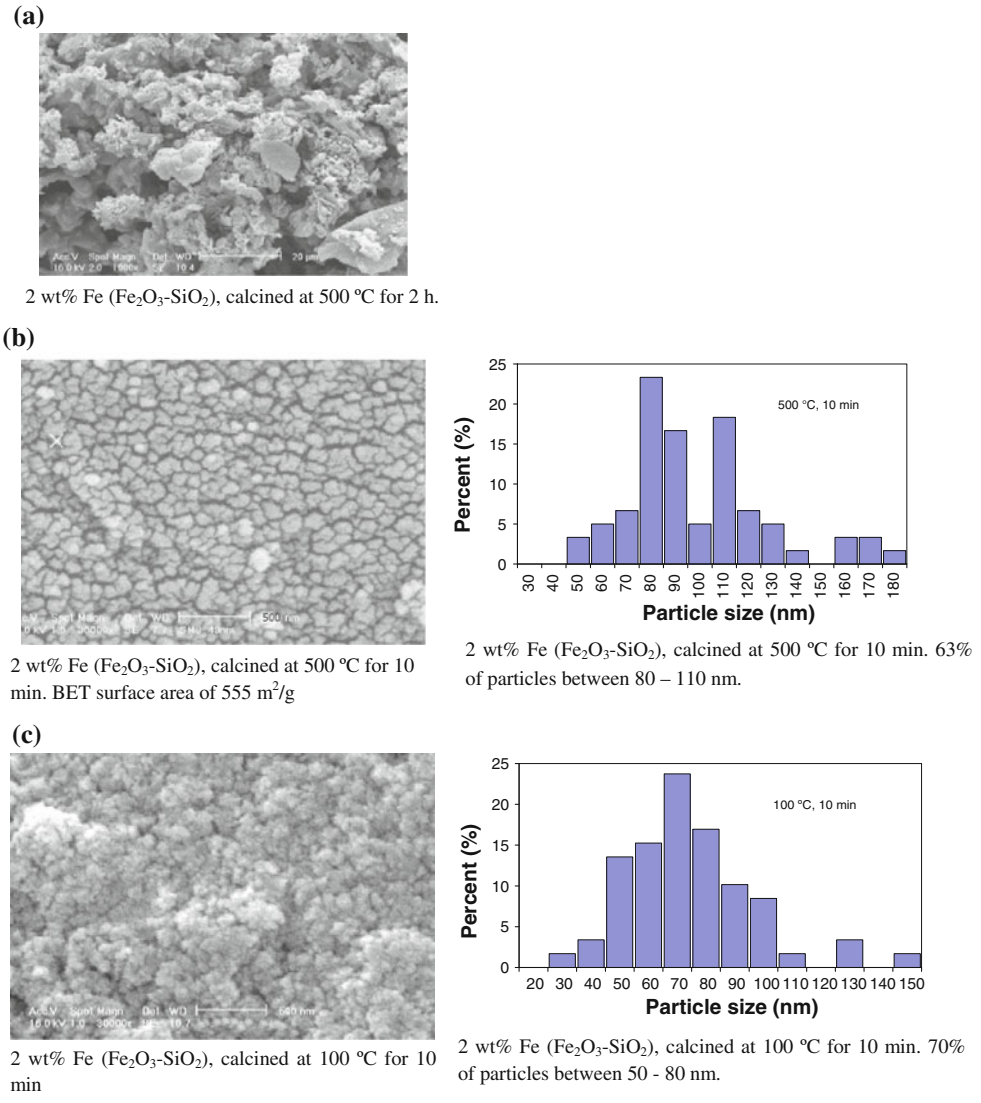

Fig. 1 SEM micrographs for the 2 wt% Fe (Fe_2O_3–SiO_2) precursor calcined **a** at 500 °C for 2 h, **b** at 500 °C for 10 min, and **c** at 100 °C for 10 min

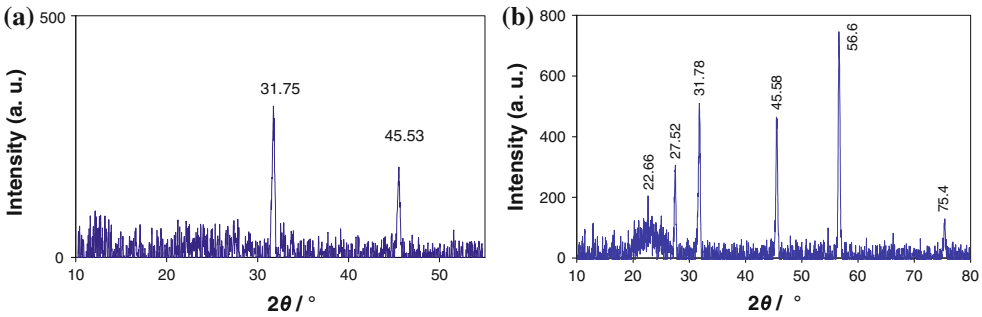

Fig. 2 XRD patterns of aerogels after being treated at 500 °C for 10 min, **a** 4.35 wt% Fe (Fe_2O_3–SiO_2), and **b** 9.6 wt% Fe (Fe_2O_3–SiO_2)

FT-IR was used for the understanding of the relation between silicon and iron in the metal oxide–silica composites. The FT-IR spectrum of Fe_2O_3–SiO_2 (**1**) is shown in Fig. 3. The bands at 3,431 and 1,624 cm^{-1} (not shown) are assignable to the ν(O–H) mode of (H-bonded) and δ(O–H) mode of water molecules, respectively. The characteristic antisymmetric (ν_{as}) Si–O–Si vibration band [43] of the [SiO_4] unit is observed around 1,074 cm^{-1} in Fe_2O_3–SiO_2 (**1**). The band at 797 cm^{-1} is assignable ν_s(Si–O–Si) modes. The small shoulder band at 966 cm^{-1} is assignable to ν(Si–OH). The band around 966 cm^{-1} observed in Fe_2O_3–SiO_2 (**1**) sample is attributed to the incorporation of the Fe^{3+} ion into the silica structure forming Si–O–Fe bonds. Note that the latter band normally appears as a sharp

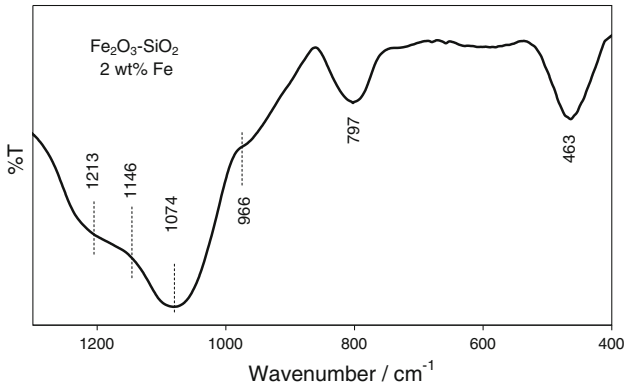

Fig. 3 FT-IR spectrum of Fe_2O_3–SiO_2 (**1**)

one in the absence of Fe_2O_3 [11]. This may indicates that the presence of Fe^{3+} affects the behavior of surface (Si–OH) groups. The incorporation of iron into the silica framework leads to a lowering of the local symmetry of the nearest neighbor [SiO_4] unit [41]. This creates a new band around 1,074 cm^{-1} which is lower in energy than the undisturbed [SiO_4] unit vibration. The v_{as}(Si–O–Si) peak for the Fe_2O_3–SiO_2 (**1**) material is seen at 1,074 cm^{-1}, 31 cm^{-1} lower than that observed for the pure SiO_2 aerogel at 1,105 cm^{-1} [15]. The same behavior was observed in the FT-IR spectra of different silicate materials [15, 44, 45]. The bending vibration band of O–Si–O bond [46] is found around 463 cm^{-1} in Fe_2O_3–SiO_2 (**1**). These FT-IR results suggest that the iron atoms are not covalently bonded to silicon in the silica network.

Catalytic activity studies

Oxidation of cyclohexanol

Oxidation of cyclohexanol was performed as a model substrate using 30% aqueous hydrogen peroxide in the presence of Fe_2O_3–SiO_2 (**1**) at 60 °C in acetonitrile. The results are depicted in Table 2. It is noteworthy that in blank experiments (entries 1–3), no significant oxidation was observed under similar reaction conditions in the absence of H_2O_2 and catalyst **1** and only a low conversion (3%) was observed in the presence of 40 μmol imidazole after prolonged (24 h) reaction times (Table 2, entry 2). Cyclohexanol was oxidized by H_2O_2/Fe_2O_3–SiO_2 to give cyclohexanone as the sole product. In addition to the catalyst, the presence of a nitrogenous base (imidazole) as a cocatalyst increased dramatically the conversion of cyclohexanol from 24 to 80% after 24 h (Table 2, entries 4 and 5).

Table 2 Catalytic oxidation of cyclohexanol by H_2O_2

Entry	Catalyst	Cocatalyst	Oxidant	Conversion (%)	
				After 3 h	After 24 h
1	Fe_2O_3–SiO_2	Imidazole	None	0	0
2	None	Imidazole	H_2O_2	0	3
3	SiO_2	Imidazole	H_2O_2	0	6
4	Fe_2O_3–SiO_2	None	H_2O_2	9	24
5	Fe_2O_3–SiO_2	Imidazole	H_2O_2	27	80

Cyclohexanol 1.0 mmol, catalyst Fe_2O_3–SiO_2 (**1**) 10 mg (3.6 μmol Fe^{3+}), toluene 0.1 g, imidazole 40 μmol, acetonitrile 3 mL, H_2O_2 14 mmol at 60 ± 1 °C

Nature of oxidant and concentration

Other parameters for suitable reaction conditions to achieve the maximum oxidation of cyclohexanol such as the oxidant concentration (moles of oxidant per moles of cyclohexanol), solvent, and temperature of the reaction were investigated. The effect of oxidant and concentration on the oxidation of cyclohexanol is illustrated in Fig. 4. Different oxidant/cyclohexanol molar ratios (2:1, 4:1 and 8:1) were considered while the ratio of cyclohexanol (1.0 mmol) to catalyst (0.01 g) in 3 mL of acetonitrile at 60 ± 1 °C was constant. In this study, the oxidation of cyclohexanol was examined using various oxidants such as NaOCl, H_2O_2, *tert*-butylhydroperoxide (TBHP), and H_2O_2/urea (UHP). All the oxidants except TBHP oxidized cyclohexanol to cyclohexanone with 100% selectivity. The product yield increased by increasing the oxidant concentration. With 8 equivalents of oxidant, maximum yield was observed for TBHP followed by H_2O_2 whereas NaOCl and H_2O_2/Urea were found to be less effective for the oxidation. Aqueous hydrogen peroxide was selected by considering its high selectivity, atom economy, and environmentally benign properties.

The conversion of cyclohexanol increased with increasing the amount of hydrogen peroxide in the reaction

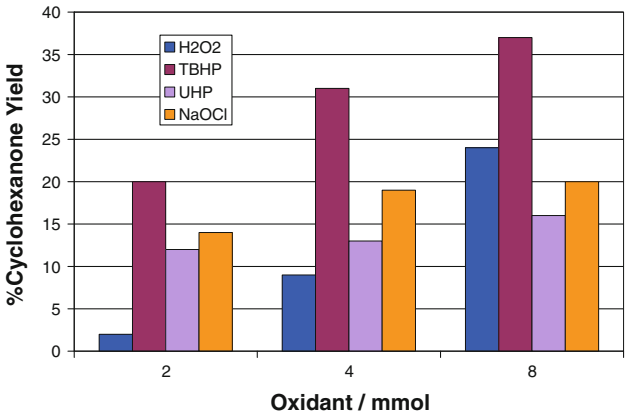

Fig. 4 Effects of concentration and nature of oxidant on the oxidation of cyclohexanol by Fe_2O_3–SiO_2 (**1**). cyclohexanol 1.0 mmol, catalyst Fe_2O_3–SiO_2 (**1**) 10 mg (3.6 μmol Fe^{3+}), toluene 0.1 g, imidazole 40 μmol, acetonitrile 3 mL, temperature 60 ± 1 °C and 5 h

mixture. When H_2O_2/substrate mole ratio was about 14, the maximum conversion of 42% was obtained (not shown in Fig. 4), showing that *ca.* 13 equivalents of the oxidant are decomposed in the non-productive way. This is, however, much less than the decomposition of hydrogen peroxide by unsupported transition metals [32, 33]. Oxidant requirement of this order in epoxidation reactions is documented in the literature [47, 48].

Effect of co-solvent

Figure 5 illustrates the influence of the co-solvent in the catalytic oxidation of cyclohexanol by Fe_2O_3–SiO_2 (**1**). Ethyl acetate, dichloromethane, acetonitrile, chloroform, dimethyl formamide, and carbon tetrachloride were used as solvents. Of the various solvents examined, acetonitrile was found to be the most suitable solvent for the reaction. The highest conversion was obtained in acetonitrile, 14% in the absence of imidazole and 42% in the presence of imidazole (see below). It was observed that the catalytic activity of the catalyst (**1**) decreased in order acetonitrile > CCl_4 > chloroform > DMF > dichloromethane > ethyl acetate in the absence of imidazole and acetonitrile > dichloromethane > DMF > chloroform > $CCl_4 \approx$ ethyl acetate in the presence of imidazole. The reactivity of catalyst **1** in other solvents was very much lower than acetonitrile (dielectric constant $\varepsilon/\varepsilon_0 = 36$ and donor number DN = 14.1 [49]) and was almost to the same extent. From Fig. 5, one could see that co-solvents with lower donation ability and high polarities seemed to favor this reaction. Solvents with high coordinating property such as DMF ($\varepsilon/\varepsilon_0 = 36.7$ and DN = 24) inhibited this reaction. When using DMF/imidazole as solvent, 10% of cyclohexanone product was gained.

Effect of the temperature

In order to get the best reaction temperature, the reaction mixture was stirred at various temperatures (for results see Fig. 6). The cyclohexanone yield increased when the reaction was carried out at higher temperatures. With Fe_2O_3–SiO_2 (**1**) as catalyst, a maximum yield of 45% was obtained after 5 h at 80 °C. The yields were almost to the same range at 60 and 80 °C.

Effect of the cocatalyst

Hydrogen peroxide is a widely used oxidant with high active oxygen content [50, 51], but it is a rather slow oxidizing agent in the absence of activators. According to some reports, the addition of some alkaline species (e.g., NaOH, KOH, $NaHCO_3$) into the reaction system was beneficial to alkene oxidation [52–54]. The efficiency of iron-catalyzed oxygenation of hydrocarbons by hydrogen peroxide increases in the presence of amines [55]. In addition, the significant effect of imidazole as a cocatalyst in increasing substrate oxidation by non-heme systems has been reported [56]. The effect of ligands like imidazole in improving Mn–porphyrin mediated epoxidation is especially noteworthy [57, 58], and the role of imidazole in catalytic oxidation by Mn–porphyrin/H_2O_2 systems has been established [59]. It has been proved that both direct coordination of imidazole to the active manganese center (proximal effect) and its action as a base (distal effect) may facilitate the heterolytic cleavage of the O–O bond in [(porphrin)Mn^{III}–O–OH] species.

An additive like $NaHCO_3$ was not effective in cyclohexanol oxidation by Fe_2O_3–SiO_2 (**1**), but addition of a base like imidazole increased the conversion from 24 to 80% for cyclohexanol (Table 2, entries 4 and 5). The effect

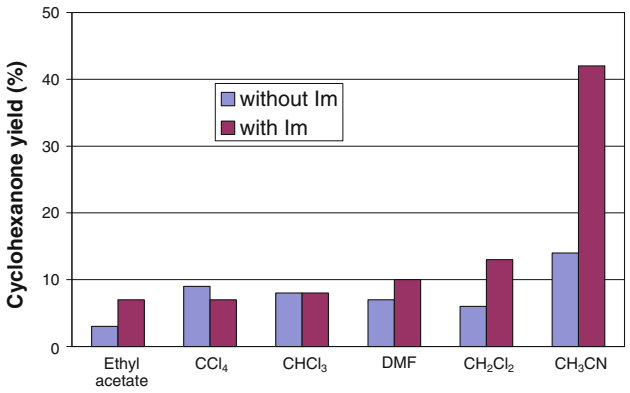

Fig. 5 Effect of solvent on the oxidation of cyclohexanol by Fe_2O_3–SiO_2 (1). *Reaction conditions*: cyclohexanol 1.0 mmol, catalyst Fe_2O_3–SiO_2 (**1**) 10 mg (3.6 μmol Fe^{3+}), toluene 0.1 g, solvent 3 mL, H_2O_2 14 mmol, imidazole (Im) 40 μmol, and temperature 60 ± 1 °C

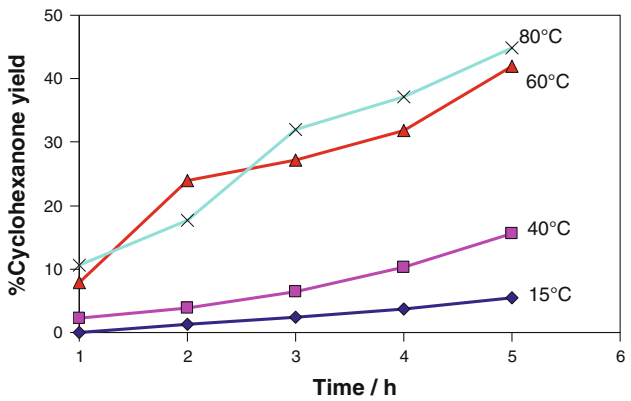

Fig. 6 Effect of temperature on conversion of cyclohexanol by Fe_2O_3–SiO_2 (1). *Reaction conditions*: cyclohexanol 1.0 mmol, catalyst Fe_2O_3–SiO_2 (1) 10 mg (3.6 μmol Fe^{3+}), toluene 0.1 g, imidazole 40 μmol, and acetonitrile 3 mL, H_2O_2 14 mmol

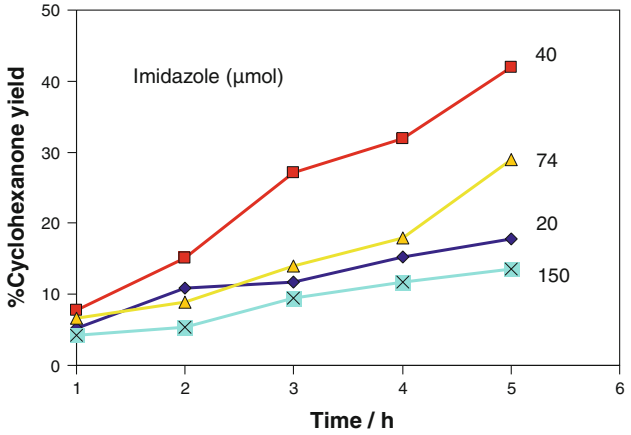

Fig. 7 Effect of imidazole concentration on oxidation of cyclohexanol by Fe_2O_3–SiO_2 (1). Reaction conditions: cyclohexanol 1.0 mmol, catalyst Fe_2O_3–SiO_2 (1) 10 mg (3.6 μmol Fe_3+), toluene 0.1 g, acetonitrile 3 mL, H_2O_2 14 mmol, and temperature 60 ± 1 °C

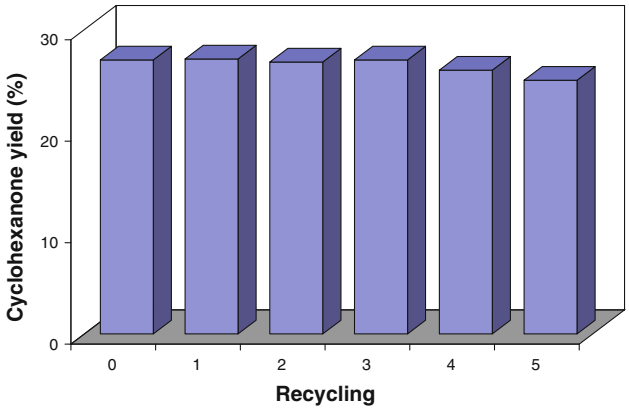

Fig. 8 Recycling studies performed with catalyst 2 wt% of Fe (Fe_2O_3–SiO_2) (1) in the oxidation of cyclohexanol by hydrogen peroxide, after 3 h of reaction time. Reaction conditions: catalyst 10 mg, cyclohexanol 1 mmol, CH_3CN 3 mL, H_2O_2 14 mmol, and temperature 60 ± 1 °C. Yields were based on the starting cyclohexanol

of the imidazole concentration on the oxidation of cyclohexanol is illustrated in Fig. 7. Different imidazole amounts (20, 40, 74, and 150 μmol) were considered while keeping the fixed amount of cyclohexanol (1 mmol) and composite (0.01 g) in 3 mL of acetonitrile at 60 ± 1 °C. Increasing the imidazole amount from 20 to 40 μmol increased the conversion from 17.8 to 42%. A higher concentration of imidazole reduced the conversion. The maximum cyclohexanol conversion was obtained with an amount of 40 μmol. We used an imidazole amount of 40 μmol in further studies. In addition, in oxidation of cyclohexanol by Fe_2O_3–SiO_2/H_2O_2 in the presence of the radical trap *tert*-butanol (10 equiv), the cyclohexanol conversion decreased from 33 to 18%. One could conclude that some part of the oxidation reaction proceeds via the hydroxyl radical. It has been assumed that imidazole facilitates proton abstraction from a H_2O_2 ligand coordinated to the iron and facilitates the catalytic cycle of generating hydroxyl radicals (and also the other possible active species) from the hydrogen peroxide. Hydroxyl radicals then attack alcohol molecules finally yielding the ketone [55]. We can assume that the role of imidazole is proton transfer (via protonation–deprotonation steps of the N-atom). The direct coordination of imidazole to the active Fe^{III} center is excluded since the solvents with high coordinating property such as DMF did not improve the oxidation yield (Fig. 5).

Catalyst recycling

Tests on catalyst recycling were carried out on Fe_2O_3–SiO_2 (**1**). The solutions remained colorless during the course of oxidations, and there was no evidence for leaching of the catalyst Fe_2O_3 from Fe_2O_3–SiO_2 (**1**) into solution. To confirm this finding in another experiment, after 5 h vigorous stirring of the oxidation mixture, the solid catalyst was removed by filtration. Cyclohexanol and H_2O_2 were added to the filtrate, and the reaction was followed for 5 h. No product was detected. This experiment also confirmed that Fe_2O_3–SiO_2 (**1**) is stable and Fe_2O_3 does not leach. The absence of Fe in the solution through leaching of **1** was also studied by measuring iron in solution. The investigation of the resulting solution by UV–Vis spectroscopy in the presence of thiocyanate showed no detectable iron. This ensured that no leaching of the active supported Fe(III) components occurred. Thus, the obtained catalytic results derive exclusively from the heterogeneous catalyst. This feature of the catalyst made it possible to remove the stable catalyst by simple filtration at the end of reaction. In order to investigate the stability and the possibility of several recycling runs for catalyst **1**, the solid catalyst was separated from the reaction mixture by filtration after the reaction, washed exhaustively with acetonitrile, and used again in a fresh reaction. The catalyst was recycled five times for cyclohexanol oxidation, and the results are seen in Fig. 8. In general, no substantial loss in the activity of the catalyst was observed compared with that of fresh sample, as shown in Fig. 8. The reused catalyst displayed consistent reactivity and selectivity.

Effect of catalyst iron content

Table 3 presents a summary of all composites evaluated as catalysts for this work. The weight percent of iron is given as the sample composition. Increasing the concentration from 2 up to 9.6 wt% increased the conversion from 42 to 59.9% but the amount of cyclohexanone produced per mole of Fe (TON) decreased. An increase in catalyst loading

Table 3 Oxidation of cyclohexanol with hydrogen peroxide under different iron content catalysts

Entry	Calcination	Catalyst	% conversion	TON[a]
1	500 °C, 10 min	2 wt% of Fe–Fe_2O_3–SiO_2	42	117
2	500 °C, 2 h	2 wt% of Fe–Fe_2O_3–SiO_2	35.6	99
3	500 °C, 10 min	4.35 wt% of Fe–Fe_2O_3–SiO_2	53	68
4	500 °C, 10 min	9.6 wt% of Fe–Fe_2O_3–SiO_2	59.9	35

Cyclohexanol 1.0 mmol, catalyst 10 mg, toluene 0.1 g, imidazole 40 μmol, acetonitrile 3 mL, H_2O_2 14 mmol, temperature 60 ± 1 °C, and reaction time 5 h

[a] *TON* turnover number = number of moles of product formed per mole of Fe in the catalyst

(Table 3, entry 4) did not cause a lowering of yield or chemoselectivity.

Oxidation of alcohols

The oxidation potential of the composite was further explored by performing oxidation of various alcohols under the same reaction conditions which proved to be the best for cyclohexanol. The Fe_2O_3–SiO_2 nanocomposite catalysts were found to exhibit excellent activity for the oxidation of a variety of alcohols using hydrogen peroxide as oxidant at 80 °C in acetonitrile, and the results are shown in Table 4. The estimated turnover numbers (TON) have also been given for each investigated alcohol. The selectivity to the corresponding carbonyl product was between 54 and 100%. Even though the best conditions and therefore the maximum conversions obtainable for individual alcohols were not optimized, the method was found to be useful in the oxidation of various primary, secondary, aliphatic, alicyclic, and aromatic alcohols. Both activated and non-activated alcohols were converted to the corresponding carbonyls efficiently. Primary alcohols all worked well under our conditions. Methanol was oxidized quantitatively to formic acid (Table 4, entry 1) and ethanol to acetaldehyde (Table 4, entry 2). The oxidation products of primary alcohols 1-pentanol and 1-heptanol (Table 4, entries 4 and 5) were the corresponding secondary alcohol and methyl alkyl ketones. The activity of secondary alcohol 2-heptanol is more than primary 1-heptanol (Table 4, entries 5 and 6). Conversion was increased for the chloro-substituted benzyl alcohol (Table 4, entry 10). Alicyclic alcohols such as cyclohexanol (Table 4, entry 7) and cyclooctanol (entry 8) were also successfully converted to their respective cyclic ketones with 100% selectivity. The oxidation products of 2-heptanol were the corresponding carbonyl product and an alcohol with rearrangement of the starting material. The unusual alcohol products obtained from the rearrangement of 1-pentanol, 1-heptanol, and 2-heptanol were also confirmed by NMR and GC by using authentic samples. For these substrates, reactions were carried out on a larger scale

Table 4 Oxidation of various alcohols catalyzed by (9.6 wt% Fe) Fe_2O_3–SiO_2/Imidazole/H_2O_2

Entry	Substrate	Alcohols conv. (%)	Product (selectivity, %)[a]	TON[b]
1	MeOH[d]	100	Formic acid (100)	58
2	EtOH[d]	100[c]	Acetaldehyde (100)	58
3	2-Propanol	100[c]	Acetone (100)	58
4	1-Pentanol	100[c]	2-Pentanol (22), 2-pentanone (78)	58
5	1-Heptanol	85	2-Heptanol (46), 2-heptanone (54)	49
6	2-Heptanol	100[d]	3-Heptanol (31), 2-heptanone (69)	58
7	Cyclohexanol	79	Cyclohexanone (100)	46
8	Cyclooctanol	54	Cyclooctanone (100)	31
9	Benzyl alcohol	94[c]	Benzaldehyde (100)	55
10	4-Chlorobenzylalcohol	100[c]	4-Chlorobenzaldehyde (100)	58
11	Cinnamyl alcohol	100[c]	Cinnamaldehyde (100)	58

Catalyst (9.6 wt% Fe) Fe_2O_3–SiO_2 10 mg (17.2 μmol), imidazole 40 μmol, alcohol 1.0 mmol, acetonitrile 3 mL, H_2O_2 14 mmol, reaction time 5 h, and reaction temperature 80 ± 1 °C. Conversions and yields are based on the starting substrate

[a] All products were identified by comparison of their physical and spectral data with those of authentic samples or GC-Mass

[b] *TON* turnover number = number of moles of product formed per mole of Fe in the catalyst sample

[c] Reaction time = 4 h

[d] 3 mmol

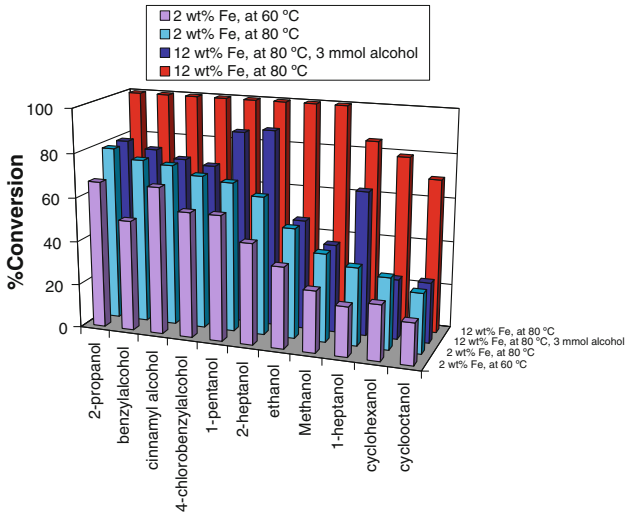

Fig. 9 Effects of the temperature, the extent of the composite iron content, and starting alcohol concentration on alcohol conversion. For reaction conditions see Table 4

and the products were isolated as further confirmation of identity and yield by NMR.

In Fig. 9, effects of the reaction temperature, amount of the composite iron content, and starting alcohol concentration on alcohol conversion are shown diagrammatically. The same effects and trend that was observed for cyclohexanol (Fig. 6; Table 3) are also seen for various alcohols.

A comparison of Fe_2O_3-SiO_2 catalytic system with previously reported systems (Table 5) shows that the conversions (especially primary alcohols) are much higher than in the other systems like vanadium phosphorus oxide catalyst [60], furthermore over-oxidation of benzyl alcohol or primary alcohols that have been reported by catalyst $SiW_{11}Zn$ [61] was not observed.

Conclusion

Silica aerogel–iron oxide nanocomposites have been prepared and are very efficient catalysts for chemoselective oxidation of various alcohols with aqueous H_2O_2. The presence of a cocatalyst like imidazole increased the catalyst efficiency enormously. The catalysts are very stable and could be easily recovered and reused without loss of activity. Although iron(III) ions decompose H_2O_2 instantly [32, 33], one remarkable property of these supported Fe_2O_3 catalysts is their ability to retard H_2O_2 decomposition to a great extent. Silica aerogel–iron oxide nanocomposite systems are highly active, selective, simple, and safe to operate. We anticipate that the present heterogeneous catalytic systems would be potentially applicable to practical organic synthesis.

Experimental

Materials

Anhydrous $FeCl_3$ and sodium from Merck and tetraethyl orthosilicate (TEOS) from Fluka were used as starting materials. Other used chemicals were isopropanol, ethanol, nitric acid, and acetylacetone (Fluka). The oxidant was 30% hydrogen peroxide (Merck). Substrates and solvents were purchased from Merck. All chemicals were of highest grade and used without further treatment.

Table 5 Comparison of the activity of heterogeneous transition metal catalysts in the oxidation of benzyl alcohol with H_2O_2

Catalyst	Product	Time (h)	Conv. (%)	Selectivity (%)	Ref.
Fe_2O_3–SiO_2	Benzaldehyde	3	94	100	This work
Cr(III)-Schiff base/MCM-41	Benzaldehyde	4	45	100	[62]
[Cu(tetraazamacrocycle)]/NaY[a]	Benzaldehyde	6	27	96.3	[63]
Ammonium molybdate	Benzaldehyde	5	77	99	[64]
Alkali-treated ZSM-5 zeolite[b]	Benzaldehyde	4	53	86	[65]
[Co($(OH)_2$-salen)]/MWNTs[c]	Benzoic acid	6	86	100	[66]
YCu(dmgH)$_2$[d]	Benzaldehyde	8	30	100	[67]
$[(n\text{-}C_4H_9)_4N]_4H[PW_{11}Ni(H_2O)O_{39}]$[e]	Benzaldehyde	12	96	37	[68]
Nanoiron oxide (Nano-γ-Fe_2O_3)	Benzaldehyde	12	33	97	[69]
Vanadium silicate xerogel (V_2O_5-SiO_2)	Benzaldehyde	24	18	100	[70]

[a] [Cu{Me_4(Bzo)$_2$[14]tetraeneN_4}]-NaY

[b] 25ZSM(AT-0.5), where 25 denotes the SiO_2/Al_2O_3 ratio and 0.5 denotes the alkali-treatment time

[c] H_2[($(OH)_2$-salen)] = *N*,*N*′-bis(4-hydroxysalicylidene)-ethylene-1,2-diamine), *MWNTs* modified multiwall carbon nanotubes

[d] *dmgH* dimethylglyoxime synthesized in situ in Y zeolite

[e] Nickel-substituted polyoxotungstate

Methods

Specific surface area was determined using a single point Brunauer–Emmett–Teller (BET) method with N_2 at 298 K on a Belsorp Mini Π apparatus. X-ray powder diffraction analysis was performed using an X'Pert diffractometer operating with Cu Ka Ni-filtered radiation, a graphite monochromator, and a proportional counter with a pulse height discriminator. IR spectra were recorded in KBr disks with a Matson 1000 FT-IR spectrophotometer. ^{1}H NMR spectra of oxidation products in DMSO-d_6 solution were recorded on a Bruker 250 MHz spectrometer. The reaction products of oxidation were determined and analyzed by HP Agilent 6890 gas chromatograph equipped with a HP-5 capillary column (phenyl methyl siloxane 30 m × 320 μm × 0.25 μm) and gas chromatograph–mass spectrometry (Hewlett-Packard 5973 Series MS-HP gas chromatograph with a mass-selective detector). The exact amount of iron in the composites was determined by ICP model ARL 3410.

Synthesis of Fe(OPr)$_3$

Sodium (0.25 g) was dissolved in 50 mL of anhydrous isopropanol under N_2 atmosphere with vigorous stirring. When complete dissolution was attained, 0.162 g (1.0 mmol) of $FeCl_3$ was added to the solution and the mixture was stirred for 120 min. A clear solution of $Fe(OPr)_3$ in isopropanol was separated by centrifugation, dried in vacuum, and the obtained solid was dissolved in 20 mL of isopropanol.

Preparation of aerogels under acidic conditions

In a typical procedure, a solution of acetylacetone (acacH, 2.0 mmol), i-PrOH (3 mL), and $Fe(OPr)_3$ (20.0 mL, acac/$Fe(OPr)_3$ 2:1 molar ratio) was heated under reflux for 1 h under N_2 with stirring. The modified iron precursor and the support precursor TEOS (9.8 mL) were dissolved in *i*-PrOH (10 mL). A hydrolyzing solution consisting of distilled water (6 mL) and concentrated nitric acid (0.27 mL) diluted in i-PrOH (6 mL) was added dropwise to the alkoxides solution under vigorous stirring. After 90 min, the final solution was transferred into a Teflon-lined autoclave for solvent evaporation. The autoclave was heated to 150 °C and kept at the final temperature for 5 h to ensure complete thermal equilibration. All as-synthesized gels were divided into small particles and calcined at 500 °C in air for 10 min to obtain 2 wt% of Fe (sample **1** Fe_2O_3–SiO_2). The overall yield per batch production was about 2.79 g, 89 wt%. The same conditions but increasing the amount of iron precursor was chosen for the preparation of samples with 4.35 wt% (sample **2** Fe_2O_3–SiO_2) and 9.6 wt% of Fe (sample **3** Fe_2O_3–SiO_2) and characterized by the techniques such as scanning electron microscopy (SEM), X-ray powder diffraction (XRD), and N_2 adsorption isotherm.

Catalytic oxidation procedures

Catalytic oxidation of alcohols was performed under air (atmospheric pressure) in 25 mL round-bottomed flasks equipped with a condenser and a small magnetic bar. The catalyst (0.01 g), substrate (1 mmol), internal standard (toluene, 0.10 g), solvent (acetonitrile, 3 mL), and aqueous H_2O_2 30% (2–14 mmol) were placed in the flask. The reaction flasks were placed in an oil bath at constant temperature (15–80 °C), while an external magnetic stirrer ensured agitation. Reactions were carried out for 5 h, under magnetic stirring. At appropriate intervals, aliquots were removed and quantified immediately by GC. The oxidation products were identified by comparing their retention times with those of authentic samples or alternatively by ^{1}H NMR and GC-mass analyses. Yields were based on the added alcohols and were determined by a calibration curve. Control reactions were carried out in the absence of catalyst, under the same conditions as the catalytic runs. No products were detected.

Each experiment was repeated three times and conversions for single experiments varied within ±2%.

Acknowledgments The authors thank the Zanjan University for the financial support of this study.

References

1. Cornell RM, Schwertmann U (1996) The iron oxides. VCH, Germany
2. Raj K, Moskovitz R (1990) J Magn Magn Mater 85:223
3. Levy L, Sahoo Y, Kim KS, Berrgey EJ, Prasad PN (2002) Chem Mater 14:3715–3721
4. Machala L, Zboril R, Gedank A (2007) J Phys Chem B 111:4003–4018
5. Nakamura T, Yamada Y, Yano K (2006) J Mater Chem 16: 2417–2419
6. Ennas G, Musinu A, Piccaluga G, Zedda D, Gatteschi D, Sangregorio C, Stanger JL, Concas G, Spano G (1998) Chem Mater 10:495–502
7. Marchetti SG, Cagnoli MV, Alvarez AM, Gallegos NG, Bengoa JF, Yeramian AA, Mercader RC (1997) J Phys Chem Solids 58: 2119–2125
8. Yi DK, Lee SS, Ying JY (2006) Chem Mater 18:2459–2461
9. Sato S, Takahashi R, Sodesawa T, Tanaka R (2003) Bull Chem Soc Jpn 76:217–223
10. Solzi M (1993) Fundamental properties of nanostructured materials. D. Fiorani and G. Sberveglieri, London
11. Khalil KMS, Makhlouf SA (2008) Appl Surf Sci 254:3767–3773
12. Dai Z, Meiser F, Möhwald H (2005) J Colloid Interface Sci 288:298–300
13. Tongpool R, Jindasuwan S (2005) Sens Actuators B 106:523–528
14. Fabrizioli P, Bürgi T, Baiker A (2002) J Catal 206:143–154
15. Clapsaddle BJ, Gash AE, Satcher JH Jr, Simpson RL (2003) J Non-Cryst Solids 331:190–201

16. Wang CT, Ro SH (2005) Appl Catal A 285:196–204
17. Savii C, Popovici M, Enache C, Subrt J, Niznansky D, Bakardzieva S, Caizer C, Hrianca I (2002) Solid State Ionics 151:219–227
18. Alcalá MD, Real C (2006) Solid State Ionics 177:955–960
19. Battishaa IK, Afify HH, Hamada IM (2005) J Magn Magn Mater 292:440–446
20. Bogatyrev VM, Guńko VM, Galaburda MV, Borysenko MV, Pokrovskiy VA, Oranska OI, Polshin EV, Korduban OM, Leboda R, Skubiszewska-Zieba J (2009) J Colloid Interface Sci 338: 376–388
21. Fernández van Raap MB, Sanchez FH, Leyva AG, Japas ML, Cabanillas E, Troiani H (2007) Physica B 398:229–234
22. Martínez S, Meseguer M, Casas L, Rodríguez E, Molins E, Moreno-Maňas M, Roig A, Sebastián RM, Vallribera A (2003) Tetrahedron 59:1553–1556
23. Sheldon RA, Kochi JK (1981) Metal-catalyzed oxidation of organic compounds. Academic Press, New York
24. Hudlicky M (1990) Oxidations in organic chemistry. ACS, Washington, DC
25. Pybus DH, Sell CS (eds) (1999) The chemistry of fragrances. RSC Paperbacks, Cambridge
26. Fey T, Fischer H, Bachmann S, Albert K, Bolm C (2001) J Org Chem 66:8154–8159
27. Sheldon RA, Arends IWCE, Dijkman A (2000) Catal Today 57:157–166
28. Griffith WP, Joliffe JM (1991) Dioxygen activation and homogeneous catalytic oxidation. Elsevier, Amsterdam
29. Ley SV, Norman J, Griffith WP, Marsden SP (1994) Synthesis 25:639–666
30. Arends IWCE, Sheldon RA (2002) Top Catal 19:133–141
31. Warner PT, Warner JC (1998) Green chemistry theory and practice. Oxford University Press, New York
32. Cotton FA, Wilkinson G (1988) Advanced inorganic chemistry, 5th edn. Wiley, New York, p 458
33. Hosseini Monfared H, Amouei Z (2004) J Mol Catal A Chem 217: 161–164
34. Hosseini-Monfared H, Ghorbani M (2001) Monatsh Chem 132: 989–992
35. Hosseini-Monfared H, Ghadimi M (2003) J Chem Res S 313–314
36. Tatibouët JM (1997) Appl Catal A Gen 148:213–252
37. Wang CT, Willey RJ (2001) J Catal 202:211–219
38. Noyori R, Aoki M, Sato K (2003) Chem Commun 16:1977–1986
39. Cannas C, Gatteschi D, Musinu A, Piccaluga G, Sangregorio C (1998) J Phys Chem B 102:7721–7726
40. Kim GJ, Kim SH (1999) Catal Lett 57:139–143
41. Fabrizioli P, Bürgi T, Burgener M, Van Doorslaer S, Baiker A (2002) J Mater Chem 12:619–630
42. Armelao L, Granozzi G, Tondello E, Colombo P, Principi G, Lottici PP, Antonioli G (1995) J Non-Cryst Solids 192–193: 435–438
43. Lippincott ER, Van Volkenburg A, Weir CE, Bunting EN (1958) J Res Natl Bur Stand 61:61–70
44. Cui H, Zayat M, Levy D (2009) J Alloys Compd 474:292–296
45. Cui H, Zayat M, Levy D (2005) Chem Mater 17:5562–5566
46. Niznansky D, Rehspringer JL (1995) J Non-Cryst Solids 180: 191–196
47. Lane BS, Vogt M, DeRose VJ, Burgess K (2002) J Am Chem Soc 124:1946–1954
48. Ueno S, Yamaguchi K, Yoshida K, Ebitani K, Kaneda K (1998) Chem Commun 295–296
49. Huheey JE (1983) Inorganic chemistry: principles of structure and reactivity, 3rd edn. Harper and Row Publisher Inc, New York, p 340
50. Sheldon RA (1993) Top Curr Chem 164:21–34
51. Schumb WC, Satterfield CN, Wentworth RL (1955) Hydrogen peroxide. Reinhold, New York
52. Rode CV, Nehete UN, Dongare MK (2003) Catal Commun 4:365–369
53. Adam W, Rao PB, Degen HG, Saha-Mller CR (2000) J Am Chem Soc 122:5654–5655
54. Lu XH, Xia QH, Zhan HJ, Yuan HX, Ye CP, Su KX, Xu G (2006) J Mol Catal A Chem 250:62–69
55. Shul'pin GB, Golfeto CC, Süss-Fink G, Shul'pina LS, Mandelli D (2005) Tetrahedron Lett 46:4563–4567 and references therein
56. Pouralimardan O, Chamayou AC, Janiak C, Hosseini-Monfared H (2007) Inorg Chim Acta 360:1599–1608
57. Gross Z, Ini S (1997) J Org Chem 62:5514–5521
58. Collman JP, Brauman JI, Fitzgerald JP, Hampton PD, Naruta Y, Michida T (1988) Bull Chem Soc Jpn 61:47–57
59. Battioni P, Renaud JP, Bartoli JF, Reina-Artiles M, Fort M, Mansuy D (1988) J Am Chem Soc 110:8462–8470
60. Pillai UR, Sahle-Demessie E (2004) Appl Catal A 276:139–144
61. Wang J, Yan L, Li G, Wang X, Ding Y, Suo J (2005) Tetrahedron Lett 46:7023–7027
62. Wang X, Wu G, Wei W, Sun Y (2010) Transition Met Chem 35:213–220
63. Kumar V, Thankachan BPP, Prasad R (2010) Appl Catal A 381:8–17
64. Chaudhari MP, Sawant SB (2005) Chem Eng J 106:111–118
65. Jia A, Lou LL, Zhang C, Zhang Y, Liu S (2009) J Mol Catal A Chem 306:123–129
66. Salavati-Niasari M, Bazarganipour M (2009) Transition Met Chem 34:605–612
67. Xavier KO, Chacko J, Mohammed Yusuff KK (2004) Appl Catal A 258:251–259
68. Kanjina W, Trakarnpruk W (2009) Silpakorn U Science & Tech J 3:7–12
69. Shi F, Tse MK, Pohl MM, Radnik J, Brückner A, Zhang S, Beller M (2008) J Mol Catal A Chem 292:28–35
70. Neumann R, Levin-Elad M (1995) Appl Catal A 122:85–97